

The precision of slow-roll predictions for the CMBR anisotropies

Jérôme Martin

*DARC, Observatoire de Paris,
UMR 8629 CNRS, 92195 Meudon Cedex, France.
e-mail: martin@edelweiss.obspm.fr*

Dominik J. Schwarz

*Institut für Theoretische Physik,
Wiedner Hauptstraße 8 – 10, 1040 Wien, Austria.
e-mail: dschwarz@hep.itp.tuwien.ac.at
(May 19, 2000)*

Inflationary predictions for the anisotropy of the cosmic microwave background radiation (CMBR) are often based on the slow-roll approximation. We study the precision with which the multipole moments of the temperature two-point correlation function can be predicted by means of the slow-roll approximation. We ask whether this precision is good enough for the forthcoming high precision observations by means of the MAP and Planck satellites. The error in the multipole moments due to the slow-roll approximation is demonstrated to be bigger than the error in the power spectrum. For power-law inflation with $n_s = 0.9$ the error from the leading order slow-roll approximation is $\approx 5\%$ for the amplitudes and $\approx 20\%$ for the quadrupoles. For the next-to-leading order the errors are within a few percent. The errors increase with $|n_s - 1|$. To obtain a precision of 1% it is necessary, but in general not sufficient, to use the next-to-leading order. In the case of power-law inflation this precision is obtained for the spectral indices if $|n_s - 1| < 0.02$ and for the quadrupoles if $|n_s - 1| < 0.15$ only. The errors in the higher multipoles are even larger than those for the quadrupole, e.g. $\approx 15\%$ for $l = 100$, with $n_s = 0.9$ at the next-to-leading order. We find that the accuracy of the slow-roll approximation may be improved by shifting the pivot scale of the primordial spectrum (the scale at which the slow-roll parameters are fixed) into the regime of acoustic oscillations. Nevertheless, the slow-roll approximation cannot be improved beyond the next-to-leading order in the slow-roll parameters.

PACS numbers: 98.80.Cq, 98.70.Vc

I. INTRODUCTION

High quality measurements of the Cosmic Microwave Background Radiation (CMBR) anisotropies have been published recently by the balloon borne experiments BOOMERanG [1] and MAXIMA-1 [2]. A large number of multipoles ($26 \leq l \leq 625$ for BOOMERanG and $36 \leq l \leq 785$ for MAXIMA-1) has been covered by both experiments. During the next years, high precision measurements will be performed by the MAP and Planck satellites [3]. Inflation [4] provides a mechanism to produce the primordial fluctuations of space-time and matter [5–8], which lead to the CMBR anisotropies and to the large scale structure. This mechanism rests on the principles of General Relativity and Quantum Field Theory. It thus can be expected to get a hand on the physics of the very early Universe with help of the upcoming high precision measurements.

The CMBR anisotropies are most conveniently expressed by the multipole moments C_l . The computation of the multipole moments requires the knowledge of the primordial spectrum and the transfer functions. The latter depend on the cosmological parameters $H_0, \Omega_M, \Omega_\Lambda, \dots$. The transfer function characterizes the

evolution of cosmological perturbations during the radiation and matter epochs. The primordial spectrum is predicted by inflation and depends on the evolution of the long wavelength perturbations during inflation and reheating. It can be predicted from a given model of inflation.

In this article, we will restrict our considerations to slow-roll inflation with one scalar field. This represents only a first step towards a more general study. Our aim is to address the following problems: What is the precision of the predicted multipole moments from the slow-roll approximation? Is this precision sufficient to reach the level of accuracy expected from the planned observations? Can the slow-roll approximation be improved to arbitrary precision?

So far, the precision of the predicted power spectrum has been examined by Grivell and Liddle [9]. However, the power spectrum is not directly observable whereas the C_l 's are. We show that the error from the slow-roll approximation is important in the multipole moments. It is bigger than the error in the power spectrum. It turns out that the next-to-leading order slow-roll approximation [10] is compulsory, but it may not be sufficient to reach an accuracy of a few % or less.

Wang, Mukhanov and Steinhardt [11] have shown that predictions based on the time delay argument [7] or on the horizon crossing/Bessel function approach (i.e. the slow-roll approximation) [10,12] are not reliable for general models of inflation. There have been various attempts to improve the slow-roll approximation to higher orders, see e.g. [10,13,14,12]. The conclusion of Wang et al. [11] has been contested by Copeland et al. [15]: “We ... conclude that any theoretical errors from the use of the slow-roll equations are likely to be subdominant”. We show in this work that this claim is not correct unless the slow-roll parameters are extremely small. Typically, we find that the slow-roll parameters must be less than 0.01 in order for the next-to-leading order to reach the level of precision of MAP or Planck. This means that there are models where the slow-roll error is dominant and the slow-roll approximation is valid. We find in agreement with the analysis in [11] that a slow-roll approximation that goes beyond the next-to-leading order cannot exist. All higher order corrections are thus meaningless. In the derivation of this result we close a gap in the proof of the next-to-leading order equations. For some reason this gap was not noticed before in the literature. For this purpose we use and generalize a new family of exact solutions, which was recently found by Starobinsky [16].

The scope of this paper is to quantify the error from the slow-roll approximation. We compute the scalar multipole moments and the ratio $R \equiv C_2^T/C_2^S$ for power-law inflation for which the exact result is known. Then, we calculate the same quantities for the same model but in the context of the slow-roll approximation. The comparison of the two results provides an estimate of the error made by using the slow-roll approximation. We do not convolute this error with the uncertainties in the transfer functions. For the sake of clarity and simplicity we only make use of the transfer functions in the long wavelength limit. This approximation only mildly affects the estimates of the error in the multipole moments. Then, we compare the slow-roll errors at leading and next-to-leading order to the cosmic variance. Binning several multipoles together allows to reduce the cosmic variance, but does not reduce the slow-roll error. We find that the slow-roll error is hidden in the cosmic variance only for very small values of the slow-roll parameters ($< 10^{-2}$). We propose to reduce the slow-roll error by optimizing the pivot scale (the scale at which the slow-roll parameters are fixed) of the spectrum. However, this method is not sufficient to hide entirely the slow-roll error in the cosmic variance.

This article is organized as follows: in the next section, the theory of cosmological perturbations and the calculations of the CMBR anisotropies are reviewed. Then, the low- l multipole moments are computed exactly for power-law inflation (Sec. III) and approximately for slow-roll inflation (Sec. IV). Comparison of the two results allows us to test the precision of the CMBR multipoles obtained from the slow-roll approximation in the last section. The slow-roll errors are shown to be observationally signifi-

cant by comparing them with the cosmic variance. We set $c = \hbar = 1$ throughout the paper.

II. FROM QUANTUM FLUCTUATIONS TO CMBR ANISOTROPIES

The line element for the spatially flat Friedmann-Lemaitre-Robertson-Walker background plus perturbations can be written as [8]:

$$ds^2 = a^2(\eta) \{ -(1 - 2\phi)d\eta^2 + 2(\partial_i B)dx^i d\eta + [(1 - 2\psi)\delta_{ij} + 2\partial_i \partial_j E + h_{ij}]dx^i dx^j \}. \quad (1)$$

In this equation, the functions ϕ , B , ψ and E represent the scalar sector whereas the tensor h_{ij} , satisfying $h_i{}^i = h_{ij}{}^{,j} = 0$, represents the gravitational waves. There are no vector perturbations because a single scalar field cannot seed rotational perturbations. The conformal time η is related to the cosmic time t by $dt = a(\eta)d\eta$. It is convenient to introduce the background quantity $\gamma(\eta)$ defined by $\gamma \equiv -\dot{H}/H^2$, where a dot means differentiation with respect to cosmic time and H is the Hubble rate, $H \equiv \dot{a}/a$. Using conformal time we may write $\gamma = 1 - \mathcal{H}'/\mathcal{H}^2$, where $\mathcal{H} \equiv a'/a$, and a prime denotes differentiation with respect to the conformal time.

We assume that inflation is driven by a single scalar field. For the perturbations we introduce gauge-invariant variables [17,8], which reduce the equations of motion, in the small scale limit, to equations of harmonic oscillators [18–21,8]. In the tensor sector (which is gauge invariant) we define the quantity μ_T for each mode k according to $h_{ij} = (\mu_T/a)Q_{ij}(k)$, where $Q_{ij}(k)$ are the (transverse and traceless) eigentensors of the Laplace operator on the spacelike sections and k^2 is the corresponding eigenvalue. Gravitational waves do not couple to scalar fields. Thus the equation of motion is given by [18]:

$$\mu_T'' + \left[k^2 - \frac{a''}{a} \right] \mu_T = 0. \quad (2)$$

The scalar sector is gauge dependent and the scalar perturbations of the metric are coupled to the perturbations of the stress tensor describing the matter. Fluctuations in the stress tensor involve perturbations in the energy density, $\delta\rho$, and in the four velocity, $\delta u^\mu = (-\phi/a, v^i/a)$. We describe perturbations in the density contrast by the gauge invariant quantity $\delta \equiv \delta\rho/\rho + (\rho'/\rho)(B - E')$. Perturbations in the velocity can be written as $v_i \equiv \partial_i w + w_i$. Since we are interested in the scalar sector, only the first term has to be taken into account. We choose to work with the gauge invariant quantity $v \equiv w + E'$. Scalar perturbations of the geometry can be characterized by the two gauge invariant Bardeen potentials $\Phi Q \equiv \phi + (1/a)[(B - E')a]'$ and $\Psi Q \equiv \psi - \mathcal{H}(B - E')$ [17], where $Q(k)$ is a scalar harmonic. During inflation, the Universe is dominated by the scalar field $\varphi = \varphi_0(\eta) + \varphi_1(\eta)Q$. Fluctuations in the scalar field are characterized by the

gauge invariant quantity $\delta\varphi \equiv \varphi_1 + \varphi'_0(B - E')$. In this simple case, the time evolution of fluctuations can be reduced to the study of the equation of motion for the variable $\mu_S \equiv -\sqrt{2\kappa} a[\delta\varphi + (\varphi'_0/\mathcal{H})\Phi]$, where $\kappa \equiv 8\pi G$. Its equation of motion is very similar to that of the gravitational waves [19,20]:

$$\mu_S'' + \left[k^2 - \frac{(a\sqrt{\gamma})''}{(a\sqrt{\gamma})} \right] \mu_S = 0. \quad (3)$$

The integration of (2) and (3) leads to the primordial spectrum of the fluctuations. For the initial conditions we assume that the scalar and tensor perturbations are in the quantum vacuum state when the scale of interest was well within the Hubble radius ($1/k_{\text{ph}} \ll c/H$) during the early stages of inflation. Therefore all fluctuation variables are quantum operators during inflation. After inflation, the Universe is filled with baryons, photons, neutrinos and (cold) dark matter. For that epoch, the perturbed Einstein equations cannot be reduced to the simple form of Eqs. (2) and (3) and need to be integrated numerically. This leads to the transfer functions.

The cosmological perturbations induce anisotropies in the temperature of the CMBR, which have been detected by COBE [22] first. This is the Sachs-Wolfe effect [23]. Since it does not depend on the photon frequency, the black body shape of the photon spectrum is conserved from the last scattering surface to its observation today [24]. The measured anisotropies in the photon intensity translate into anisotropies in the temperature of the black body.

For the temperature fluctuations we introduce the abbreviation $\Delta(\vec{e}) \equiv (\delta T/T)(\vec{e})$, where \vec{e} characterizes the direction of the beam on the celestial sphere. The contributions of the scalar and tensor perturbations are given by:

$$\Delta^S(\vec{e}) = \frac{1}{4}\delta_\gamma + \Phi - e^i \partial_i v + \int_{\eta_{\text{SS}}}^{\eta_0} d\bar{\eta} \frac{\partial}{\partial \bar{\eta}} (\Phi + \Psi), \quad (4)$$

$$\Delta^T(\vec{e}) = -\frac{1}{2}e^i e^j \int_{\eta_{\text{SS}}}^{\eta_0} d\bar{\eta} \frac{\partial}{\partial \bar{\eta}} h_{ij}. \quad (5)$$

The first three terms of the scalar contribution are evaluated on the last scattering surface, i.e. at η_{SS} . They represent the intrinsic fluctuations, the Sachs-Wolfe effect and the Doppler effect. The fourth term is the so-called integrated Sachs-Wolfe effect. The integration is performed along the photon trajectory, which is parameterized by the conformal time here. η_0 denotes the conformal time at observation today. δ_γ is the perturbed density contrast of the photons and v the perturbed velocity of the photon fluid. For large angular scales only the first two terms are important. For isentropic (sometimes called adiabatic) perturbations the scalar part reduces to:

$$\Delta^S(\vec{e}) = \frac{1}{3}\Phi(\vec{e}) + (\dots). \quad (6)$$

Usually, the CMBR anisotropies are expressed through the multipole moments C_l . The C_l are the coefficients in

an expansion over Legendre polynomials of the CMBR temperature two-point correlation:

$$\langle \Delta^{S,T}(\vec{e}_1) \Delta^{S,T}(\vec{e}_2) \rangle = \frac{1}{4\pi} \sum_l (2l+1) C_l^{S,T} P_l(\cos \delta), \quad (7)$$

where $\cos \delta \equiv \vec{e}_1 \cdot \vec{e}_2$. The brackets $\langle \rangle$ denote the averaging over many ensembles. Averages over many ensembles cannot be replaced by spatial averages on the celestial sphere due to the lack of ergodicity of the stochastic process $\Delta(\vec{e})$, see Ref. [25]. If, nevertheless, we do this the error made can be quantified by means of the cosmic variance.

The computation of the multipoles for a given model requires the knowledge of the initial spectrum of the fluctuations and of the transfer function. The power spectrum of the Bardeen potential is defined in terms of the two-point correlator for the operator $\hat{\Phi}(\eta, \mathbf{x})$:

$$\langle 0 | \hat{\Phi}(\eta, \mathbf{x}) \hat{\Phi}(\eta, \mathbf{x} + \mathbf{r}) | 0 \rangle \equiv \int_0^\infty \frac{dk}{k} \frac{\sin kr}{kr} k^3 P_\Phi(\eta, k). \quad (8)$$

Similarly, the power spectrum of gravitational waves is defined as:

$$\langle 0 | \hat{h}_{ij}(\eta, \mathbf{x}) \hat{h}^{ij}(\eta, \mathbf{x} + \mathbf{r}) | 0 \rangle \equiv \int_0^\infty \frac{dk}{k} \frac{\sin kr}{kr} k^3 P_h(\eta, k). \quad (9)$$

A priori, the primordial power spectra are time dependent quantities. However, for the multipoles between $l = 2$ and $l = 2000$, we are interested in scales which are well beyond the horizon at the end of inflation. In a first approximation for those scales the power spectra do not evolve in time during inflation and they can be written as:

$$k^3 P_\Phi(k) = A_S^i(k_0) \left(\frac{k}{k_0} \right)^{n_S-1}, \quad (10)$$

$$k^3 P_h(k) = A_T^i(k_0) \left(\frac{k}{k_0} \right)^{n_T}, \quad (11)$$

where the spectral indices n_S , n_T and the amplitudes A_S^i , A_T^i are independent quantities and k_0 is an arbitrarily fixed scale which is introduced to link various notations in the literature. The spectral indices can also be determined from $n_S - 1 \equiv d \ln(k^3 P_\Phi) / d \ln k$ and $n_T \equiv d \ln(k^3 P_h) / d \ln k$.

An accurate calculation of the multipole moments requires numerical computations. However, for small l , the approximate equation (6) can be used. For density perturbations [26] this leads to:

$$C_l^S = \frac{4\pi}{9} \int_0^\infty \frac{dk}{k} j_l^2(kr_{\text{ISS}}) T_\Phi(kr_{\text{ISS}} \rightarrow 0) \times A_S^i \left(\frac{k}{k_0} \right)^{n_S-1}, \quad (12)$$

where j_l is the spherical Bessel function of order l and $r_{\text{ls}}^{\text{ph}} \equiv a(\eta_0)r_{\text{ls}} = a_0(\eta_0 - \eta_{\text{ls}}) \approx a_0\eta_0 \approx 2R_{\text{H}}$ is the comoving line-of-sight distance to the last scattering surface.

$T_{\Phi}(kr_{\text{ls}} \rightarrow 0)$ is approximately the transfer function for superhorizon modes. It is k independent and therefore only the amplitude is modified but not the spectral index. The domain of validity of the latter approximation can be evaluated as follows. In the integral (12) the main contribution comes from the modes around $kr_{\text{ls}} \sim l + 1$. We use that to estimate for which multipole moments the k independent transfer function is good enough. The mode whose wavelength is equal to the Hubble radius today, i.e. such that $2\pi a_0/k = l_H(\eta_0)$, has $k\eta_0 = 4\pi$. Therefore the constant superhorizon transfer function is a reasonably good approximation if $(l + 1)/r_{\text{ls}} \ll 4\pi/\eta_0$, that is to say $l \ll 10$. This is a very optimistic estimate since it does not take into account the first approximation, made in Eq. (6), on which the validity of Eq. (12) rests.

With the above approximations the low- l multipoles can be calculated exactly [26]. The result reads:

$$C_l^{\text{S}} = \pi^{3/2} \frac{\Gamma[(3 - n_{\text{S}})/2]\Gamma[l + (n_{\text{S}} - 1)/2]}{\Gamma[(4 - n_{\text{S}})/2]\Gamma[l + 2 - (n_{\text{S}} - 1)/2]} \times (k_0 r_{\text{ls}})^{1 - n_{\text{S}}} \frac{A_{\text{S}}}{9}, \quad (13)$$

where $A_{\text{S}} \equiv A_{\text{S}}^i T_{\Phi}(kr_{\text{ls}} \rightarrow 0)$. For gravitational waves we obtain the following expression [27]:

$$C_l^{\text{T}} = \frac{9\pi}{4}(l - 1)l(l + 1)(l + 2)(k_0 r_{\text{ls}})^{-n_{\text{T}}} \times \int_0^{\infty} \frac{dy}{y} |I_l(y)|^2 A_{\text{T}} y^{n_{\text{T}}}, \quad (14)$$

where the function $I_l(y)$, $y \equiv kr_{\text{ls}}$, is defined by:

$$I_l(y) \equiv \int_0^y \frac{j_2(x)j_l(y - x)}{x(y - x)^2} dx. \quad (15)$$

The superhorizon transfer function for gravitational waves does not appear explicitly because it is equal to one. As a consequence we can write $A_{\text{T}}^i \equiv A_{\text{T}}$. The computation of C_l^{T} is more complicated than the calculation of C_l^{S} . The integral I_l can be calculated exactly in terms of special functions, see Ref. [27]. However, the second integration over k cannot be performed analytically and we must rely on numerical integration.

Below we will be interested in the ratio of tensor to scalar quadrupole contributions [28–31]:

$$R \equiv \frac{C_2^{\text{T}}}{C_2^{\text{S}}}. \quad (16)$$

Expressed in terms of the tensor spectral index this is the so-called consistency equation of inflation.

We have seen that the calculation of C_l^{S} requires the knowledge of the transfer function and of the primordial

spectrum. In principle, $T_{\Phi}(kr_{\text{ls}})$ is known accurately as the result of numerical calculations, e.g. see Refs. [32]. When we calculate the multipoles using Eqs. (12) or (14) we make two approximations: a long wavelength approximation for the transfer function and we neglect the contribution of radiation (pure matter assumption) to the expansion of the Universe at photon decoupling. The long wavelength approximation results in neglecting other contributions besides (6) in the Sachs-Wolfe effect for scalars and in considering that the tensor and scalar superhorizon transfer functions are constant. The pure matter assumption results in a small error in the numerical value of $T_{\Phi}(kr_{\text{ls}} \rightarrow 0)$. However, for small values of l these errors are small.

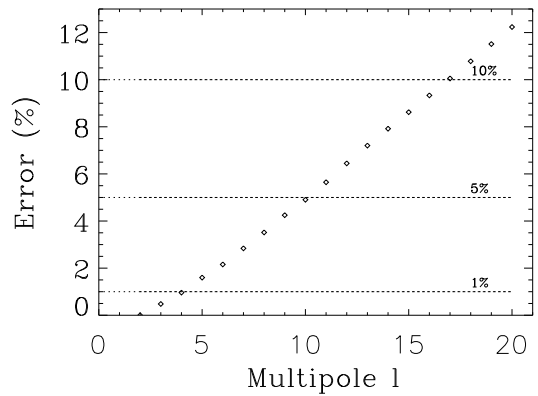


FIG. 1. Error due to the long wavelength approximation in the transfer function for the scalar multipoles with a flat primordial spectrum. The exact multipoles are calculated by means of the CMBFAST code and are normalized to the quadrupole.

In order to test this claim quantitatively and to quantify the contribution to the total error coming from the transfer function (see Fig. 1), we compute the scalar multipole moments for low l numerically with CMBFAST [33] for the following values of the cosmological parameters: $H_0 = 50 \text{ km/s/Mpc}$, $\Omega_0 = 1$, $\Omega_{\text{CDM}} = 0.95$, $\Omega_{\text{B}} = 0.05$. We compare them to the multipole moments given by Eq. (12) with a constant transfer function. The code CMBFAST automatically normalizes to the COBE result [22]. The result is expressed by the band powers $(\delta T_l/T_0)^2 \equiv l(l + 1)C_l/(2\pi)$, where $T_0 \approx 2.73 \text{ K}$ is the average temperature of the CMBR. For a flat ($n_{\text{S}} = 1$) primordial spectrum, CMBFAST gives $\delta T_2 \approx 27.5 \mu\text{K}$ or $Q_{\text{rms-PS}} \approx 17.8 \mu\text{K}$, where the quadrupole rms fluctuation is given by $Q_{\text{rms-PS}} \equiv T_0 \sqrt{(5/4\pi)C_2}$. We normalize the amplitude A_{S} in Eq. (12) is to the latter value of the quadrupole. In Fig. 1 we plot the differences of both calculations, divided by the CMBFAST results, and express this number as the error in %. The error in the quadrupole (13) vanishes “by construction”. Equation (12) shows

that $\delta T_l = T_0 \sqrt{A_S} / 3 (k_0 r_{\text{ISS}})^{(1-n_S)/2} = Q_{\text{rms-PS}} \sqrt{12/5}$, whereas the CMBFAST- δT_l is l -dependent, despite both band powers are calculated from the same primordial spectrum. The difference between both band powers is exclusively due to the use of different transfer functions and to the neglect of the Doppler and integrated Sachs-Wolfe effects. In this way, we can isolate and estimate the error coming from the long wavelength approximation, being given that the spectrum is normalized to COBE.

A similar study has been done in Ref. [34]. The errors given in that article differ from those obtained here because a different normalization is used. In Ref. [34], the spectrum is normalized to the multipole moment C_{10} instead of the quadrupole. As a consequence, in that case the error in C_{10} vanishes “by construction”.

Figure 1 confirms the importance of the transfer function and the analytical estimates made at the beginning of this article. The error is below 1% only for $l < 4$. For C_{10} , which is often used to normalize the spectrum, the effect of the subleading terms in k is already 5%. The error from the pure matter assumption has not been fully accounted for by this method, because we do not test the error in the numerical value of $T_\Phi(kr_{\text{ISS}} \rightarrow 0)$ when we normalize the quadrupole to the COBE result. Since this error is a pure overall numerical factor, it does not affect our conclusions.

III. PREDICTIONS OF POWER-LAW INFLATION

In this section, we turn to the study of power-law inflation. This model is of particular importance because it allows to calculate all quantities of interest exactly. Moreover, this exact result is at the basis of the slow-roll approximation.

Power-law inflation is given by the following solution for the scale factor and the scalar field:

$$a(\eta) = l_0 |\eta|^{1+\beta}, \quad \varphi = \varphi_i + \frac{m_{\text{Pl}}}{2} \sqrt{\frac{\gamma}{\pi}} (1+\beta) \ln |\eta|, \quad (17)$$

where m_{Pl} is the Planck mass and φ_i is the initial value of the scalar field at conformal time η_i . In this model inflation occurs if $\beta < -2$ (we do not consider the case where $-2 < \beta < -1$ which cannot be realized with a single scalar field). The quantity l_0 has the dimension of a length and its value will roughly determine the amplitude of the CMBR fluctuations today. In the particular case of power-law inflation, the function $\gamma(\eta)$ is a constant equal to $(2+\beta)/(1+\beta)$. For $-\infty < \beta < -2$, γ goes from one to zero, this last value corresponding to the de Sitter spacetime. The scale factor and scalar field of Eqs. (17) are solutions of the Einstein equations for the scalar field potential:

$$V(\varphi) = V_i \exp \left[\frac{4\sqrt{\pi}}{m_{\text{Pl}}} \sqrt{\gamma} (\varphi - \varphi_i) \right], \quad (18)$$

where V_i is the value of the potential at η_i .

A. Density perturbations

The effective potential for density perturbations, $U_S \equiv (a\sqrt{\gamma})''/(a\sqrt{\gamma})$, see Eq. (3), reads:

$$U_S(\eta) = \frac{(\beta+1)\beta}{\eta^2}. \quad (19)$$

This simple form of the potential allows an exact integration of Eq. (3). The solution is expressed in terms of Bessel functions. This provides the initial power spectrum, i.e. A_S^i and n_S . In order to evolve the superhorizon spectrum, we can rely on the conservation law [35,21] for the quantity: $\zeta \equiv (\mathcal{H}^{-1}\Phi' + \Phi)/\gamma + \Phi$. This gives the superhorizon transfer function: $T_\Phi(kr_{\text{ISS}} \rightarrow 0) = [9(2\beta+3)^2]/[25\gamma^2(1+\beta)^2]$. Then the amplitude of the scalar quadrupole and the spectral index take the form:

$$A_S(k_0) = \frac{l_{\text{Pl}}^2}{l_0^2} \frac{9}{25\pi\gamma} f(\beta) k_0^{n_S-1}, \quad n_S = 2\beta + 5 = \frac{1-3\gamma}{1-\gamma}, \quad (20)$$

where

$$f(\beta) \equiv \frac{1}{\pi} \left[\frac{\Gamma(-\beta-1/2)}{2^{\beta+1}} \right]^2, \quad (21)$$

which is unity for $\beta = -2$. As expected, the amplitude of scalar perturbations is roughly determined by the ratio l_{Pl}/l_0 . Very often the final spectrum is expressed in terms of the Hubble rate at some time η_* , instead of the scale l_0 . We have $H_* \equiv H(\eta_*) = -[(1+\beta)/l_0]|\eta_*|^{-2-\beta}$. Therefore the amplitude reads:

$$A_S(k_0) = l_{\text{Pl}}^2 H_*^2 \frac{9}{25\pi\gamma} f(\beta) |1+\beta|^{2(\beta+1)} \left(\frac{k_0}{a_* H_*} \right)^{n_S-1}. \quad (22)$$

The amplitude A_S is displayed as a function of γ in Fig. 2. It diverges in the de Sitter limit $\gamma \rightarrow 0$. COBE measured the spectral index to be $n_S = 1.2 \pm 0.3$ [22]. The $1(2)\sigma$ value $n_S = 0.9(0.6)$ corresponds to $\gamma \approx 0.048(0.167)$.

B. Gravitational waves

The calculation of the spectrum for gravitational waves is performed along the same lines as above. The effective potential is the same as for density perturbations, i.e. $U_T \equiv a''/a = \beta(1+\beta)/\eta^2$. Since the superhorizon transfer function is equal to one, A_T and n_T can be written as:

$$A_T(k_0) = \frac{l_{\text{Pl}}^2}{l_0^2} \frac{16}{\pi} f(\beta) k_0^{n_T}, \quad n_T = 2\beta + 4 = -\frac{2\gamma}{1-\gamma}. \quad (23)$$

For power-law inflation, the relation $n_S = n_T + 1$ holds. In terms of H_* the amplitude is given by

$$A_T(k_0) = l_{\text{Pl}}^2 H_*^2 \frac{16}{\pi} f(\beta) |1 + \beta|^{2(\beta+1)} \left(\frac{k_0}{a_* H_*} \right)^{n_T}. \quad (24)$$

Figure 2 shows the scalar and tensor amplitudes (22) and (24), respectively. For $\gamma > 9/400 = 0.0225$ the tensor mode dominates.

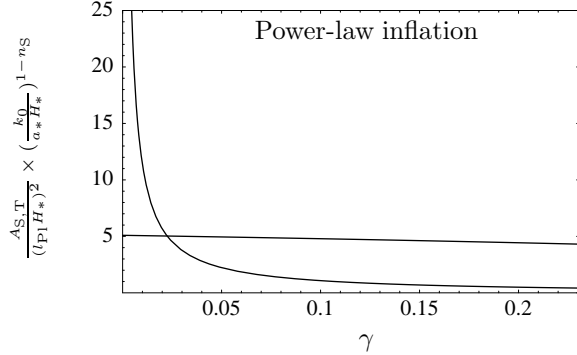


FIG. 2. The amplitudes of scalar and tensor perturbations. In the de Sitter limit $\gamma \rightarrow 0$ the scalar amplitude diverges. For larger values of γ the perturbations are dominated by the tensor mode.

C. Multipole moments

The multipole moments predicted by power-law inflation can easily be computed from Eqs. (13) and (14). The quadrupoles are displayed in Fig. 3. Compared to the amplitudes the importance of the tensor mode is slightly suppressed, it becomes the dominant mode at $\gamma \gtrsim 0.07$, which corresponds to $n_S \lesssim 0.85$.

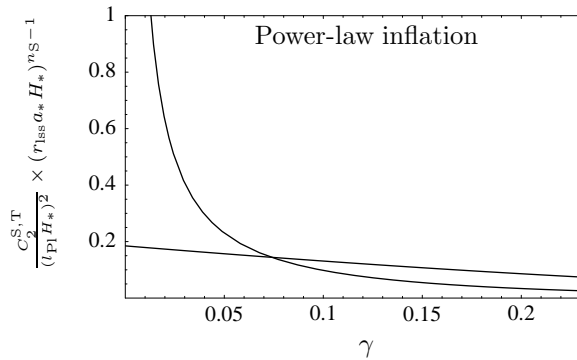


FIG. 3. The quadrupole moments of scalar and tensor perturbations.

We calculate the ratio R for power-law inflation:

$$R = 13.86\gamma F[n_T(\gamma)] = -6.93 \frac{n_T}{1 - \frac{n_T}{2}} F(n_T), \quad (25)$$

where the function $F(n_T)$ is given by:

$$F(n_T) \equiv 496.1 \times 2^{1-n_T} \frac{\Gamma^2(\frac{3-n_T}{2}) \Gamma(4 - \frac{n_T}{2})}{\Gamma(2 - n_T) \Gamma(2 + \frac{n_T}{2})} \times \int_0^\infty dk k^{n_T-1} |I_2(k)|^2. \quad (26)$$

In this expression we have used the equation $n_S = n_T + 1$, valid for power-law inflation only, to express everything in terms of n_T . We have $\int_0^\infty dk k^{-1} |I_2(k)|^2 = 2.139 \times 10^{-4}$ such that $F(n_T = 0) = 1$. Notice that the factors $k_0 r_{\text{ls}}$ and $k_0 / (a_* H_*)$ cancel in R because $n_S = n_T + 1$. R versus γ is plotted in Fig. 4. This plot demonstrates that within the 2σ error bars of COBE, there is a large parameter space where the tensor mode dominates the scalar modes, see e.g. Refs. [29,31] for a more detailed discussion.

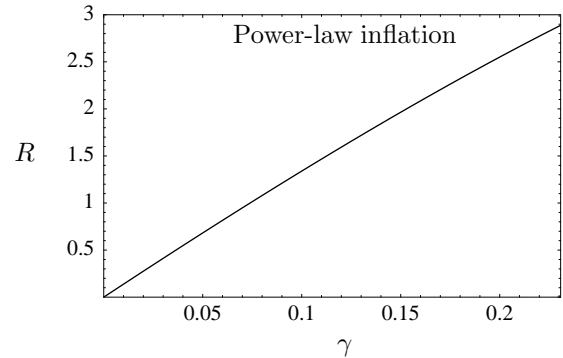


FIG. 4. The tensor to scalar ratio of the quadrupole moments.

IV. PREDICTIONS OF SLOW-ROLL INFLATION

For a general model of inflation exact solutions are not available. Generically, the potentials U_S and U_T are different but nevertheless their shape is similar. A sketch of the generic form of U_S and U_T is displayed in Fig. 5. The details of the realistic reheating transition are not taken into account in this simple figure. During the radiation dominated era the potential goes to zero, since $a \propto \eta$.

For a given mode k , the inflationary epoch can be divided into three stages, see Fig. 5. In region I the mode k is subhorizon. In that case the effective potential is small compared to k^2 . In the limit $k/(aH) \rightarrow \infty$ for fixed k , the vacuum fluctuations are given by, see Ref. [21]:

$$\mu_{S,T}(\eta) \rightarrow \mp 4\sqrt{\pi} l_{\text{Pl}} \frac{e^{-ik(\eta-\eta_i)}}{\sqrt{2k}}, \quad (27)$$

respectively. In region III the mode is superhorizon. In the limit $k/(aH) \rightarrow 0$ at fixed k , the potential term is dominant, and the “exact” solutions read:

$$\begin{aligned} \mu_S(\eta) &= C_S(a\sqrt{\gamma})(\eta) \times \\ &\left[1 - k^2 \int^\eta \frac{1}{(a^2\gamma)(\tilde{\eta})} \int^{\tilde{\eta}} (a^2\gamma)(\tilde{\eta}) d\tilde{\eta} d\tilde{\eta} \right], \quad (28) \\ \mu_T(\eta) &= C_T a(\eta). \quad (29) \end{aligned}$$

Usually, density perturbations are described in terms of the Bardeen potential Φ instead in terms of μ_S . The order k^2 term is necessary to obtain the leading order expression for the Bardeen potential, since $\Phi = [\mathcal{H}\gamma/(2k^2)][\mu_S/(a\sqrt{\gamma})]'$, see Refs. [21,20]. Thus, in region III, the superhorizon Bardeen potential is given by:

$$\Phi(\eta) = \frac{C_S \mathcal{H}}{2a^2} \int^\eta a^2 \gamma d\bar{\eta}. \quad (30)$$

Our aim is to calculate the spectra at the end of inflation, i.e. in region III. The time dependence of the solutions in this region is known and the difficulty lies in the calculation of the constants C_S and C_T . Since the solutions are uniquely determined in region I, this amounts to join the super- and subhorizon solutions. Therefore we need to know the behavior of the perturbations in region II.

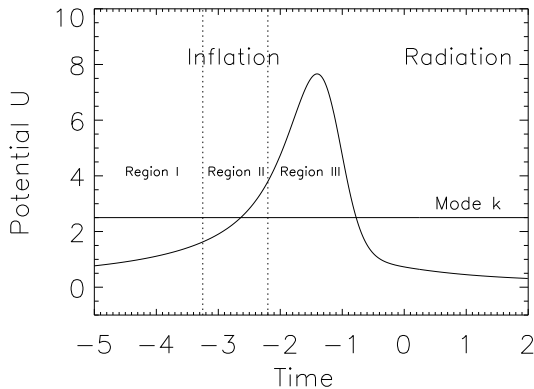


FIG. 5. Sketch of the effective potential for density perturbations and/or gravitational waves during inflation and radiation.

A popular approach is the slow-roll approximation [10,12]. The idea is that there was an epoch during inflation where the scalar field was rolling down its potential $V(\varphi)$ very slowly. Under certain conditions (see below) this is close to the behavior during power-law inflation and the exact solutions from power-law inflation are used in region II to interpolate between the sub- and superhorizon solutions.

Slow roll is controlled by the three (leading) slow-roll parameters (see e.g. Ref. [12]) defined by:

$$\epsilon \equiv 3 \frac{\dot{\varphi}^2}{2} \left(\frac{\dot{\varphi}^2}{2} + V \right)^{-1} = -\frac{\dot{H}}{H^2}, \quad (31)$$

$$\delta \equiv -\frac{\ddot{\varphi}}{H\dot{\varphi}} = -\frac{\dot{\epsilon}}{2H\epsilon} + \epsilon, \quad (32)$$

$$\xi \equiv \frac{\dot{\epsilon} - \dot{\delta}}{H}. \quad (33)$$

We see in particular that $\gamma(\eta) = \epsilon$ in region II. The equations of motion for ϵ and δ can be written as:

$$\frac{\dot{\epsilon}}{H} = 2\epsilon(\epsilon - \delta), \quad \frac{\dot{\delta}}{H} = 2\epsilon(\epsilon - \delta) - \xi. \quad (34)$$

The slow-roll conditions are satisfied if ϵ and δ are much smaller than one and if $\xi = \mathcal{O}(\epsilon^2, \delta^2, \epsilon\delta)$. From Eqs. (34), it is clear that this amounts to consider ϵ and δ as constants. This property is crucial for the calculation of the perturbations.

For power-law inflation the slow-roll parameters satisfy:

$$\epsilon = \delta < 1, \quad \xi = 0. \quad (35)$$

Therefore the slow-roll conditions are fulfilled if $\epsilon \ll 1$, that is to say if β is close to -2 (scale invariance). In fact, the slow-roll approximation is an expansion around power-law inflation with $0 < -(\beta + 2) \ll 1$. To illustrate this point, let us consider the exact equation:

$$\eta = -\frac{1}{aH} + \int da \frac{\epsilon}{a^2 H}. \quad (36)$$

If we assume that ϵ is a constant, the previous equation reduces to $aH \approx -(1 + \epsilon)/\eta$. This is equivalent to a scale factor which behaves like:

$$a(\eta) \approx l_0 |\eta|^{-1-\epsilon}. \quad (37)$$

Interestingly enough, the effective power index at leading order depends on ϵ only.

A. Density perturbations

The effective potential of density perturbations can be calculated in terms of the slow-roll parameters exactly. The result is:

$$U_S(\eta) = a^2 H^2 [2 - \epsilon + (\epsilon - \delta)(3 - \delta) + \xi]. \quad (38)$$

In the slow-roll approximation $a^2 H^2 \approx \eta^{-2}(1 + 2\epsilon)$ and the effective potential reduces to $U_S \approx (2 + 6\epsilon - 3\delta)\eta^{-2}$. Since ϵ and δ must be seen as constants in the slow-roll approximation, the equation of motion (3) is of the same type as in power-law inflation. The solutions are given by Bessel functions:

$$\mu_S = (k\eta)^{1/2} [B_1 J_{\nu_S^{(sr)}}(k\eta) + B_2 J_{-\nu_S^{(sr)}}(k\eta)], \quad (39)$$

whose order is given by

$$\nu_S^{(sr)} = -\frac{3}{2} - 2\epsilon + \delta. \quad (40)$$

A comment is in order here: The potential U_S depends on the scale factor and its derivatives only. One could think, looking at Eq. (37), that U_S also depends on ϵ only. This is not the case. The reason is that U_S contains terms like $\dot{\epsilon}/\epsilon$ (for example) which are linear in δ , see Eqs. (34). First one must calculate all derivatives, replace

them with their expression in terms of ϵ and δ , and only then consider that the slow-roll parameters are constant.

We would also like to stress that keeping higher orders in ϵ does not make sense. If terms of quadratic order in the slow-roll parameters are kept, the solution for density perturbations in region II can no longer be expressed in terms of Bessel functions. This is because the slow-roll parameters can no longer be considered as constant in time, see Eqs. (34). Therefore any considerations at this order in the framework of the slow-roll approximation is meaningless. The same conclusion has been obtained by Wang, Mukhanov, and Steinhardt [11].

Let us now calculate the constant C_S . The first step is to match the solutions of region I and II. This procedure fixes B_1 and B_2 . Using Eqs. (27) and (28), one obtains: $B_1/B_2 = -e^{i\pi\nu_S^{(sr)}}$ and $B_1 = 2i\pi l_{P1} \exp[i\nu_S^{(sr)}(\pi/2) - i(\pi/4) + ik\eta_i]/(\sqrt{k} \sin \pi\nu_S^{(sr)})$. Note that B_1 and B_2 do not depend on the time at which the matching between regions I and II is performed. The joining between regions II and III remains to be performed at some time η_S , which will be fixed below. Expanding everything up to next-to-leading order in the slow-roll parameters, one obtains:

$$|C_S|^2 = \frac{l_{P1}^2}{l_0^2} \frac{8\pi}{\epsilon} \left[1 - 2(C + \ln k)(2\epsilon - \delta) + 2(\delta - \epsilon) \ln |\eta_S| \right] k^{-3}, \quad (41)$$

with $C \equiv \gamma_E + \ln 2 - 2 \approx -0.7296$, $\gamma_E \approx 0.5772$ being the Euler constant. The Bardeen potential given in Eq. (30) is now completely specified. Note that $\gamma(\eta)$ in Eq. (30) is a time dependent function, evaluated in region III, whereas ϵ in Eq. (41) is a constant parameter, which is fixed by $\epsilon = \gamma(\eta_S)$.

For scalar perturbations it is useful to evaluate the quantity

$$\zeta = -\frac{\mu_S}{2a\sqrt{\epsilon}}, \quad (42)$$

which is a *constant* for the dominant mode at superhorizon scales [35,8,21]. The quantity $-\zeta$ is denoted \mathcal{R} in Ref. [12]. Instead of expressing the spectrum in terms of the ratio l_{P1}/l_0 , it is usual to write it in terms of the Hubble rate at some time η_* . Of course, there is nothing deep in this choice and one could have kept working with l_{P1}/l_0 . A priori, the value of η_* is arbitrary and could either be in regions I, II or III. However, in order to make contact with the literature, we will assume that η_* is in region II. Then, in the slow-roll approximation, the value of $H(\eta_*)$ can be written as:

$$H_* \equiv H(\eta_*) = \frac{1}{l_0} [1 + \epsilon(1 + \ln |\eta_*|)]. \quad (43)$$

In Ref. [12], η_* is the time which satisfies the relation $a(\eta_*)H(\eta_*) = k$ for each mode k . In other words, we have

$\eta_* = \eta_*(k)$. In this article, we adopt another convention and choose η_* such that it is not a function of k . Then, a straightforward calculation gives

$$k^3 P_\zeta(k) = \frac{l_{P1}^2 H_*^2}{\pi \epsilon} \left\{ 1 - 2\epsilon - 2[C + \ln k |\eta_*|] (2\epsilon - \delta) + 2(\delta - \epsilon) \ln \left| \frac{\eta_S}{\eta_*} \right| \right\}. \quad (44)$$

The matching time η_S remains to be fixed by a physical argument. To our knowledge, this issue has been overlooked in the literature so far. All works on the slow-roll approximation, starting with Ref. [10], have tacitly assumed that $\eta_S/\eta_* = 1$, without further justification. A priori, an equally good choice would be, for example, when the mode $a_* H_*$ crosses the effective potential, i.e. when $(1 + 2\epsilon)/\eta_*^2 = U_S(\eta_S)$. It is easy to show that this boils down to the choice $\eta_S/\eta_* = \sqrt{2}$. It is important to realize that different choices for the ratio η_S/η_* lead to different observational predictions. Although a change in η_S would not change the spectral index, it would change the amplitude of scalar perturbations and the ratio of tensor to scalar contributions R .

The missing physical argument comes from a new family of exact solutions which has a slow-roll regime in a certain limit. One exact solution is of course power-law inflation, but it does not help for the purpose of fixing η_S/η_* , because the spectrum does not depend on η_S/η_* for $\delta = \epsilon$. These solutions are found by the ansatz

$$a\sqrt{\gamma} = \frac{A}{|\eta|^\alpha}, \quad (45)$$

where A and α are two free parameters. This defines a two-parameters family of exact solution. Note that this family is not equivalent to power-law inflation. The power-law model ($A = l_0 \sqrt{\gamma(\beta)}$, $\alpha = -1 - \beta$) is a subclass of this two-parameter family. Of course, this is because $a(\eta) \propto |\eta|^{-\alpha}$ is just a solution of Eq. (45), viewed as a second order differential equation for the scale factor, but not the general solution. The limit A to zero and α close to one gives a slow-roll inflation model. The particular case $\alpha = 1$ was already found recently by Starobinsky [16]. This one parameter family of solutions is characterized by a flat spectrum, $n_S = 1$. Eq. (45) is a generalization of Starobinsky's original ansatz [16]. The spectrum may be calculated exactly to read

$$k^3 P_\zeta(k) = \frac{l_{P1}^2}{\pi^2 A^2} 2^{2\alpha} \Gamma^2 \left(\alpha + \frac{1}{2} \right) k^{-2(\alpha-1)}. \quad (46)$$

The case $\alpha = 1$ gives $k^3 P_\zeta(k) = l_{P1}^2/(\pi A^2)$ and coincides with the result of Ref. [16].

We now need to calculate the slow-roll spectrum for this new class of solutions. A comparison with Eq. (44) will allow us to fix the ratio η_S/η_* . Let us first determine the slow-roll parameters. In the slow-roll approximation we find

$$\frac{(a\sqrt{\gamma})'}{a\sqrt{\gamma}} = -\frac{1}{\eta}(1 + 2\epsilon - \delta), \quad (47)$$

whereas insertion of the ansatz (45) into this equation gives $(a\sqrt{\gamma})'/(a\sqrt{\gamma}) = -\alpha/\eta$. Therefore, one has $2\epsilon = (\alpha - 1) + \delta$ and especially $2\epsilon = \delta$ if $\alpha = 1$. It is interesting to note that we no longer have the relation $\epsilon = \delta$ typical of power-law inflation. Let us also emphasize that the two-parameter family is the only family of exact solutions which permits a slow-roll approximation. Eq. (47) is a necessary condition for the validity of the slow-roll approximation. This equation can be viewed as a first-order differential equation for the quantity $a\sqrt{\gamma}$. Integration of this equation leads to the ansatz given in Eq. (45). Therefore our determination of the ratio η_S/η_* is general. The value of A in the slow-roll limit is obtained from $A = a\sqrt{\gamma}|\eta|^\alpha$ and is expressed in terms of H_* with the help of (36). This gives $A^2 = \epsilon H_*^{-2}[1 + 2\epsilon + 2(2\epsilon - \delta) \ln |\eta_*|]$. Thus we obtain the slow roll spectrum from Eq. (46):

$$k^3 P_\zeta(k) = \frac{l_{\text{Pl}}^2 H_*^2}{\pi \epsilon} [1 - 2\epsilon - 2(C + \ln k |\eta_*|)(2\epsilon - \delta)]. \quad (48)$$

A comparison with (44) shows that

$$\eta_S = \eta_*. \quad (49)$$

Note that we could have derived the slow-roll spectrum of ζ from the exact spectrum (46) right from the beginning, by approximating it in the slow-roll regime. However, we have chosen to take the Bessel function/horizon crossing approach, because it is this approach which has been discussed in the literature. Let us note that the transfer function for ζ is unity. This means that the spectrum of ζ during the matter dominated era is identical to the spectrum at the end of inflation (region III).

We are mostly interested in the spectrum of the metric potential Φ since this quantity appears in the calculations of the multipole moments, see Eq. (12). If we assume that the Universe is matter dominated at the surface of last scattering, then the conservation law provides us with the relation $\zeta = (5/3)\Phi$. Then, the spectrum of the Bardeen potential follows from (48) as:

$$n_S^{(\text{sr})} = 1 - 4\epsilon + 2\delta, \quad (50)$$

$$A_S^{(\text{sr})} = \frac{9l_{\text{Pl}}^2 H_*^2}{25\pi \epsilon} [1 - 2\epsilon - 2(C + \ln k_0 |\eta_*|)(2\epsilon - \delta)]. \quad (51)$$

These expressions are consistent with (4.3) and (5.1) of [12]. The amplitude of scalar perturbations blows up when the slow-roll approximation becomes accurate, i.e. when ϵ goes to zero.

To end this section, let us make a last comment. It is clear from the previous considerations that we need the slow-roll approximation in region II only. In particular, this scheme of approximation is not needed in region III

since the ‘‘exact’’ solution is known. However, one may wish to use it in region III also. Then, in this region, the Bardeen potential is given by $\Phi \approx (C_S/2)\epsilon(1 - 3\epsilon + 2\delta)$. The long-wavelength transfer function, which allows to pass from the end of inflation to the matter dominated epoch can be expressed as $T_\Phi \approx [9/(25\epsilon^2)](1 + 6\epsilon - 4\delta)$. Using the two previous formula, one can show that one recovers the spectrum given in Eqs. (50) and (51). However, in principle, this method is not appropriate since we use an approximated solution whereas an exact one is available.

B. Gravitational waves

For gravitational waves, the same lines of reasoning can be applied. In region II, the effective potential can be written as:

$$U_T(\eta) = a^2 H^2 (2 - \epsilon), \quad (52)$$

and gives in the slow-roll limit

$$U_T(\eta) \sim \frac{2 + 3\epsilon}{\eta^2}. \quad (53)$$

Therefore the matching of sub- and superhorizon solution is again reduced to power-law inflation. The solution of μ_T is similar to the one given in Eq. (39), where the effective index of the Bessel function is now given by:

$$\nu_T^{(\text{sr})} = -\frac{3}{2} - \epsilon. \quad (54)$$

This solution can be used to find the constant C_T . Then, the power spectrum of gravitational waves reads

$$k^3 P_h(k) = \frac{l_{\text{Pl}}^2}{l_0^2} \frac{16}{\pi} (1 - 2C\epsilon - 2\epsilon \ln k), \quad (55)$$

from which we deduce that:

$$n_T^{(\text{sr})} = -2\epsilon, \quad (56)$$

$$A_T^{(\text{sr})} = l_{\text{Pl}}^2 H_*^2 \frac{16}{\pi} [1 - 2(C + 1 + \ln k_0 |\eta_*|)\epsilon]. \quad (57)$$

We see that there exists a crucial difference between density perturbations and gravitational waves. In the case of gravitational waves, the ambiguity related to the choice of the matching time is not present.

The amplitudes of scalar and tensor modes versus the slow-roll parameter ϵ are displayed in Fig. 6 for $\delta = \epsilon$ and in Fig. 7 for $\delta = 2\epsilon$ at leading and next-to-leading order. The first case is an approximation to the exact power-law result, the case $\delta = 2\epsilon$ is the slow-roll approximation to Starobinsky’s exact solution.

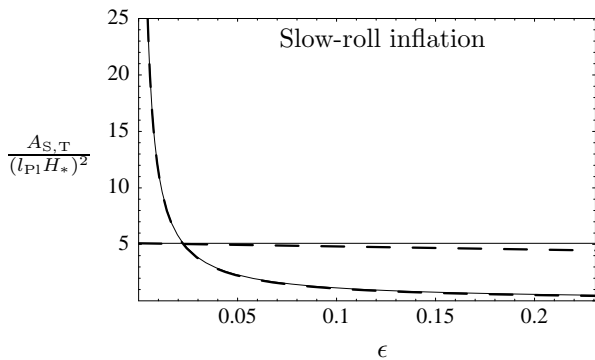


FIG. 6. The scalar and tensor amplitudes from the slow-roll approximation for $\epsilon = \delta$. The scalar amplitude diverges in the de Sitter limit $\epsilon \rightarrow 0$. The leading order is drawn by full lines, the next-to-leading order by dashed lines. We have set $k_0 |\eta_*| = 1$.

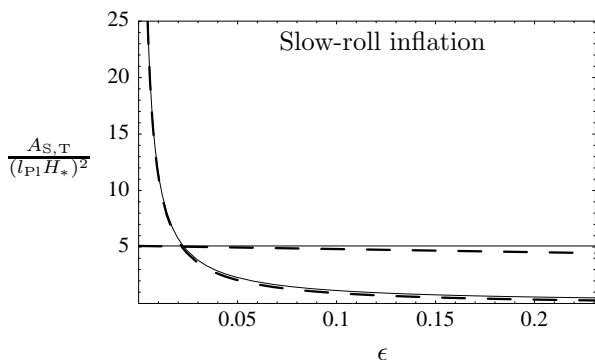


FIG. 7. The same as Fig. 6, but for $\delta = 2\epsilon$.

C. Multipole moments

Let us first start with the calculation of C_l^S . We write the scalar multipoles as

$$C_l^S \equiv g_l(n_S) \frac{A_S}{9}, \quad (58)$$

which defines the function $g_l(n_S)$, cf. Eq. (13). To compute C_l^S at the next-to-leading order in the slow-roll parameters we need to expand $g_l(n_S)$ to first order around $n_S = 1$, since n_S itself is a linear function of ϵ and δ :

$$g_l(n_S) = g_l(n_S = 1) + (n_S - 1) \frac{dg_l}{dn_S}(n_S = 1) \quad (59)$$

$$= \frac{2\pi}{l(l+1)} [1 + (n_S - 1)(D_l - \ln k_0 r_{\text{ISS}})], \quad (60)$$

where

$$D_l \equiv 1 - \ln 2 + \Psi(l) + \frac{l+1/2}{l(l+1)} \quad (61)$$

and $\Psi(x) \equiv d \ln \Gamma(x)/dx$. For the quadrupole we have $D_2 \approx 1.1463$ and for large l , $D_l = 1 + \ln(l/2) + \mathcal{O}(1/l)$, due to $\Psi(l) = \ln l + \mathcal{O}(1/l)$. Using Eqs. (50) and (51), we find the scalar multipoles at next-to-leading order as

$$C_l^S = \frac{2l_{\text{Pl}}^2 H_*^2}{25\epsilon} \frac{1}{l(l+1)} \left[1 - 2\epsilon - 2(D_l + C)(2\epsilon - \delta) + 2(2\epsilon - \delta) \ln \frac{r_{\text{ISS}}}{|\eta_*|} \right]. \quad (62)$$

In this equation the Doppler effect, the integrated Sachs-Wolfe effect, and the evolution of the transfer function are neglected. In the next section we will argue that this does not prevent the estimation of the slow-roll error.

We now calculate R in the slow-roll regime at the leading and next-to-leading order. The scalar quadrupole follows from (62) and reads:

$$C_2^S = \frac{l_{\text{Pl}}^2 H_*^2}{75\epsilon} \left[1 - 2\epsilon - 2(D_2 + C)(2\epsilon - \delta) + 2(2\epsilon - \delta) \ln \frac{r_{\text{ISS}}}{|\eta_*|} \right], \quad (63)$$

where $D_2 + C \approx 0.4167$.

Let us now compute C_2^T . Using Eqs. (14) and (57), we find at next-to-leading order

$$C_2^T = 0.1848 l_{\text{Pl}}^2 H_*^2 \left[1 - 2 \left(B + C + 1 - \ln \frac{r_{\text{ISS}}}{|\eta_*|} \right) \epsilon \right], \quad (64)$$

where the number B is defined by $B \equiv \int_0^\infty dk k^{-1} \ln(k) I_2^2(k) / \int_0^\infty dk k^{-1} I_2^2(k) \approx 1.2878$ so that $B + C \approx 0.5582$. For higher tensor multipoles the numerical values of the constants in (64) are modified, but not the functional dependence on the slow-roll parameters. In Fig. 8 the scalar and tensor quadrupoles at leading and next-to-leading orders are displayed for the case $\epsilon = \delta$.

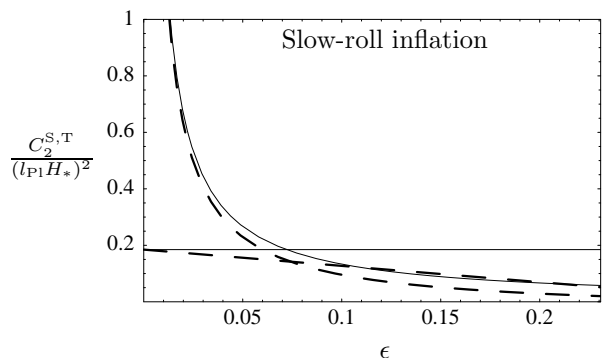


FIG. 8. The scalar and tensor quadrupole moments from the slow-roll approximation for $\epsilon = \delta$. The leading order is drawn by full lines, the next-to-leading order by dashed lines. We have set $r_{\text{ISS}} = |\eta_*|$.

Taking into account the expressions for C_2^S and C_2^T given previously, we finally find the following expression for R in the slow-roll regime:

$$R = 13.86\epsilon \left[1 + 0.5504\epsilon - 0.8334\delta - 2(\epsilon - \delta) \ln \frac{r_{\text{ISS}}}{|\eta_*|} \right]. \quad (65)$$

At leading order we recover the so-called *consistency condition for slow-roll inflation* [12], which reads

$$R = -6.93n_T. \quad (66)$$

This equation cannot be generalized by the use of (65) to a next-to-leading order equation, because it would involve the knowledge of the order $\mathcal{O}(\epsilon^2)$ terms in n_T . As discussed above, terms of that order are not meaningful in the slow-roll approximation.

In Fig. 9, the ratio R is displayed at leading and next-to-leading order for the two cases $\epsilon = \delta$ and $2\epsilon = \delta$.

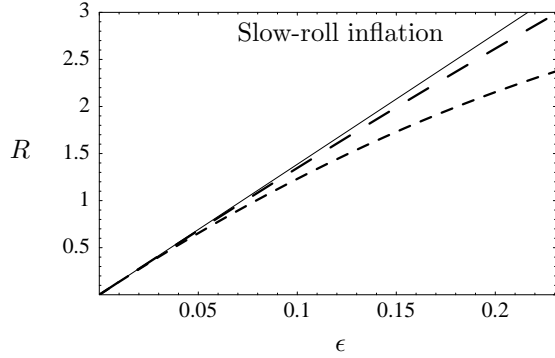


FIG. 9. The tensor to scalar ratio at leading order (full line) and at next-to-leading order for $\delta = \epsilon$ (long dashed line) and $\delta = 2\epsilon$ (short dashed line). The leading order is independent of δ . We have set $r_{\text{ISS}} = |\eta_*|$.

V. DISCUSSION OF ERRORS

The aim of this section is to quantify the magnitude of the error introduced by the slow-roll approximation. For this purpose, we compare the slow-roll predictions with the exact results of power-law inflation. We explicitly test the following quantities: $Q \in \{n_S - 1, n_T, A_S, A_T, C_I^S, C_2^T, R\}$, i.e. quantities related to the power spectra and the quadrupole moments.

We denote by Q the exact result of power-law inflation and by $Q^{(0)}$, $Q^{(1)}$ the slow-roll results at leading and next-to-leading orders, respectively. The error is estimated by calculating:

$$e_Q^{(i)} \equiv \left| \frac{Q^{(i)} - Q}{Q} \right| \times 100\%. \quad (67)$$

Let us start with an estimate of the errors in the prediction of the spectral indices n_S and n_T . For the leading

order slow-roll approximation $n_T = n_S - 1 = 0$ and thus the error is $e_{n_S-1}^{(0)} = e_{n_T}^{(0)} = 100\%$, except for de Sitter inflation. It is absolutely compulsory to use the next-to-leading order result for the spectral indices. We express the error as a function of γ . The best slow-roll approximation to a power-law model is given by $\epsilon = \delta = \gamma$, and therefore $n_T^{(\text{sr})} = n_S^{(\text{sr})} - 1$ for this case. Thus from Eqs. (20), (23), (50), and (56) the error in the spectral indices from the slow-roll approximation is

$$e_{n_S-1}^{(1)} = e_{n_T}^{(1)} = \gamma \times 100\%. \quad (68)$$

Thus the next-to-leading order slow-roll approximation predicts the spectral indices with an error less than 1%, if $\gamma < 0.01$ or $0.98 < n_S < 1$.

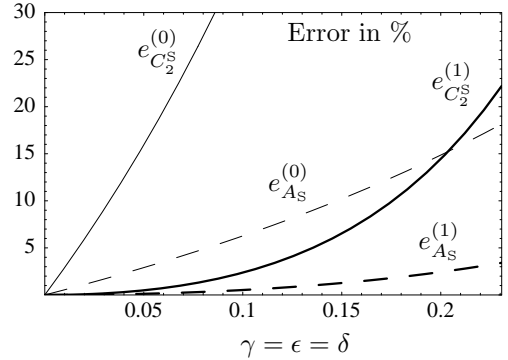


FIG. 10. The error in the scalar quantities. The full lines are the quadrupole moments, the dashed lines are the amplitudes. The thin lines are the leading order corrections, the thick lines are the next-to-leading order corrections.

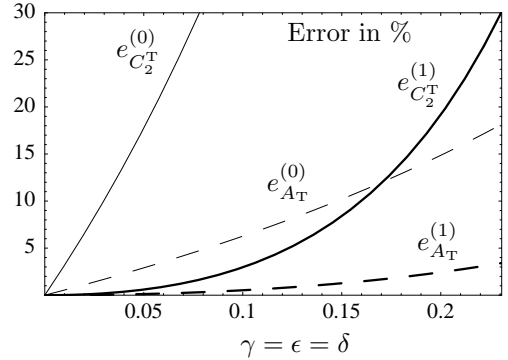


FIG. 11. The same as Fig. 10, but for the tensor amplitude and quadrupole moment. For the amplitude the error is the same as for the scalar sector, because $\epsilon = \delta$.

So far, except in some of the figures, we did not specify the pivot scale k_0 . We now choose to fix $k_0 \equiv a_* H_*$, i.e. k_0 is the mode that crosses the horizon at the time η_* , which is the time when we determine the values of the slow-roll parameters, where we fix them once and forever. It is easy to show that this amounts to take $|\eta_*| = k_0^{-1}$

in the argument of the logarithm which shows up in the equations of the previous section. Still η_* remains to be fixed, which can be done most conveniently by fixing $k_0 r_{\text{ISS}}$. In the following we will show that this choice is of physical relevance, because the accuracy of the slow-roll approximation can be improved by a clever choice of the pivot scale. We will discuss two cases. The usual convention is to choose $k_0 r_{\text{ISS}} = 1$. This corresponds to $k_0^{\text{phys}} = h/(6000 \text{ Mpc})$ today. Below we show that this leads to huge errors from the slow-roll approximation.

To improve the precision of the slow-roll approximation we suggest to minimize the error in the region of the first acoustic peak, i.e. around $l \sim 200$. For this purpose we choose a pivot scale such that $k_0 r_{\text{ISS}} \approx 100e$, which corresponds to a physical wavenumber $k_0^{\text{phys}} = h/(22 \text{ Mpc})$ today. Let us start by analyzing the errors for the pivot $k_0 = 1/r_{\text{ISS}}$.

The errors in the amplitudes and quadrupoles for the case of power-law inflation, $\epsilon = \delta$, are displayed in Figs. 10 and 11. From these two plots, we can draw three conclusions. The first conclusion is that the error in the quadrupoles is larger than the error in the amplitudes. This confirms the results already obtained in Ref. [36]. The second conclusion is that it is not possible to obtain an error at the 1% level with the leading order, except for very small values of the slow-roll parameters. The third conclusion is that the accuracy of the next-to-leading order for the quadrupoles is better than 1% if $\gamma < 0.07$, which corresponds to $0.85 < n_S$. Since the slow-roll approximation is more accurate for power-law model, it is reasonable to expect larger errors for more realistic models.

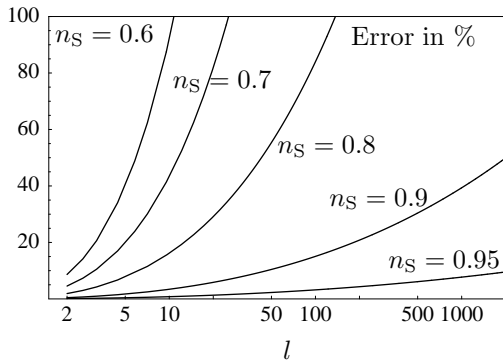


FIG. 12. The error from the next-to-leading order slow-roll approximation in the scalar multipoles C_l^S versus l for various values of the spectral index n_S . The approximation is best close to today's horizon since, in this figure, we have taken $k_0 r_{\text{ISS}} = 1$, the most common choice.

Let us now turn to the slow-roll errors in higher scalar multipole moments. Although we cannot obtain the exact result for the high- l multipole moments without making use of a Boltzmann code, we can nevertheless estimate the errors from the slow-roll approximation in this regime. As already discussed around Fig. 1 computing

the scalar multipoles from Eq. (12) is a bad approximation for high l . Despite this fact, it is clear that for a given cosmological model the transfer function is the same for a power-law model and its slow-roll approximation. Thus the only difference between the power-law and slow-roll multipole moments can arise from the convolution of this transfer function with different initial spectra. We expect that this difference is small. To put it differently, $C_l(\text{sr}, t) - C_l(\text{sr}, a)$ is large, whereas $C_l(\text{sr}, t) - C_l(\text{pl}, t) \approx C_l(\text{sr}, a) - C_l(\text{pl}, a)$, where t (a) denotes the use of the true (approximated) transfer function and sr (pl) denotes the initial spectrum. Thus we use Eqs. (13), (20), and (62) to obtain the errors for the scalar multipoles as a function of l , (67), which are displayed in Fig. 12. It shows that these errors are large and increase with l and $|n_S - 1|$.

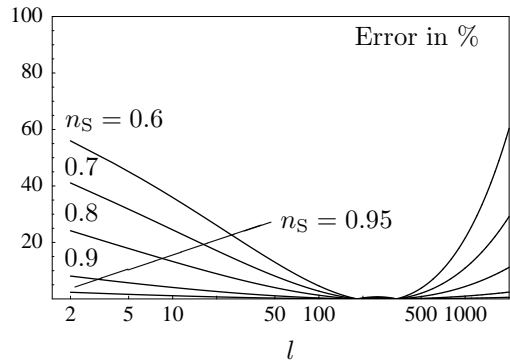


FIG. 13. The same as figure 12, but with $k_0 r_{\text{ISS}} = 100e$. This optimizes the accuracy in the region of the first acoustic peak.

The reason for the large errors in the multipole moments are the large errors in the spectral indices. This can be understood from the relations between the errors:

$$\frac{e_{C_l^S}^{(0)}}{100} = \left| \frac{g_l(1)}{g_l(n_S)} \left(1 + \frac{e_{A_S}^{(0)}}{100} \right) - 1 \right|, \quad (69)$$

$$\frac{e_{C_l^S}^{(1)}}{100} = \left| \frac{g_l(1)}{g_l(n_S)} \left(1 + \frac{e_{A_S}^{(1)}}{100} \right) + \frac{g_l'(1)(n_S - 1)}{g_l(n_S)} \right. \\ \left. \times \left(1 + \frac{e_{A_S}^{(0)}}{100} \right) \left(1 - \frac{e_{n_S-1}^{(1)}}{100} \right) - 1 \right|, \quad (70)$$

where the prime denotes a derivative with respect to n_S . The signs in front of the errors in the amplitude and in the spectral index are model dependent. For $\delta = \epsilon$ the error in the amplitude has always positive sign, the error in the spectral index has a negative sign. For small values of l we may expand

$$g_l(n_S) = g_l(1) + g_l'(1)(n_S - 1) + \mathcal{O}[(n_S - 1)^2] \quad (71)$$

in Eqs. (69) and (70). Keeping only terms linear in $n_S - 1$ and terms linear in the errors we find

$$e_{C_l^S}^{(i)} \approx e_{A_S}^{(i)} + (D_l - \ln k_0 r_{\text{ISS}})(1 - n_S)e_{n_S-1}^{(i)}, \quad (72)$$

where D_l has been introduced in Eq. (61). The error in the quadrupole moment is now easily understood from the last equation. As claimed above, the large error in the spectral index is responsible for the large error in the quadrupole moment. The contribution from the error in the spectral index always dominates. It is obvious from Fig. 12 that the error increases with l and with $|n_S - 1|$. Equation (72) underestimates the error for large l and $|n_S - 1|$, due to the breakdown of the expansion (71).

These large errors, displayed in Fig. 12, can be shifted to different multipoles by a change of the pivot scale k_0 . Therefore, one may hide part of the error from the slow-roll approximation in the cosmic variance. Inspection of Eq. (72) suggests that the error is minimized for a given multipole if $D_l = \ln(k_0 r_{\text{ISS}})$. For large l

$$k_0 \approx \frac{e}{2} \frac{l}{r_{\text{ISS}}}, \quad \text{or} \quad k_0^{\text{phys}} \approx \frac{e}{4} l H_0, \quad (73)$$

where H_0 is today's Hubble rate. We would like to know the position and height of the first acoustic peak very accurately, which suggests to choose $l_{\text{minimal error}} \approx 200$. This gives $k_0 = 1/22 h^{-1} \text{ Mpc} \approx 1/31 \text{ Mpc}$ for $h = 0.71$, the HST key project final value. Figure 13 shows the errors at the next-to-leading order for various values of the scalar index with the new choice for the pivot scale. It can be seen clearly that the errors are highly suppressed around $l \approx 200$, as expected, but increase at lower and higher multipoles. The tiny bump between $l \approx 200$ and $l \approx 500$ is due to the fact that we plot the absolute value, in this region the error changes its sign. The new choice of the pivot scale allows to predict the multipoles in the range $2 \leq l \leq 2000$ for $n_S = 0.9$ better than 10%, which was not possible with the pivot scale chosen previously. Nevertheless, the precision is not good enough to reach the 1% accuracy level (the error is 2.4% at $l = 2000$). In order to do so it is necessary to have $n_S > 0.93$ or $\gamma < 0.032$.

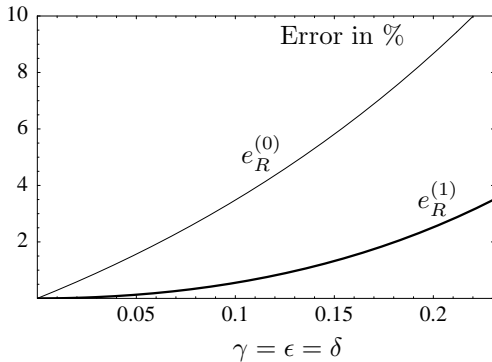


FIG. 14. The error in the tensor to scalar ratio in leading (thin line) and next-to-leading order (thick line).

The error in the T/S ratio is displayed in Fig. 14. In our special situation the pivot scale does not enter R ,

because $\epsilon = \delta$ [see Eq. (65)]. We see that the error in R is less important than for the amplitudes and/or the quadrupoles. Therefore this suggests to use R to test the single scalar field/slow-roll paradigm. However, it is clear that any violation of the consistency check by the forthcoming data should be interpreted as a failure of this paradigm but not as the failure of inflation itself. In a more general situation where $\epsilon \neq \delta$, the choice of k_0 does affect the error in R . Since we do not have an exact solution for scalar and tensors modes such that $\epsilon \neq \delta$ at our disposal, it is difficult to predict the corresponding effect.

The errors from the slow-roll approximation displayed in Figs. 10, 11, 12, and 13 should be compared with the cosmic variance. The cosmic variance is the variance of the best unbiased estimator for the multipole moments [25,37]: $\mathcal{E}_{\text{Best}}(C_l) = 1/(2l+1) \sum_{m=-l}^{m=l} a_{lm} a_{lm}^*$, where we have expanded the temperature fluctuations over the basis of spherical harmonics, $\Delta(\vec{e}) = \sum_{lm} a_{lm} Y_{lm}(\vec{e})$. This expression is valid only if the a_{lm} 's satisfy a Gaussian or a mildly non-Gaussian statistics. The corresponding error can be written as

$$e_{C_l}^{(\text{cv})} \equiv \frac{\sigma_{\mathcal{E}_{\text{Best}}(C_l)}}{C_l} \times 100\% = \sqrt{\frac{2}{2l+1}} \times 100\%. \quad (74)$$

Over the whole range of the spectrum that will be measured by a mission like Planck the cosmic variance is larger than 2% ($l \approx 2000$) and is $\approx 7\%$ at the first acoustic peak ($l \approx 200$).

It is possible to reduce the cosmic variance by binning several multipoles together at the expense of decreasing the precision on the location of the multipoles. Therefore, we define an averaged multipole, \bar{C}_l , on the range $[l-L, l+L]$ by

$$\bar{C}_l \equiv \frac{1}{2L+1} \sum_{j=l-L}^{l+L} j(j+1) C_j. \quad (75)$$

The central value l of each interval must be separated by $2L+1$. For an incomplete sky coverage L is restricted by the form of the basis used to expand $\Delta(\vec{e})$. Below we do not take this issue into account and assume that the full sky is covered. In order to calculate the cosmic variance associated with the binned multipole, we define the estimator

$$\mathcal{E}(\bar{C}_l) \equiv \frac{1}{2L+1} \sum_{j=l-L}^{l+L} \frac{j(j+1)}{2j+1} \sum_{m=-j}^j a_{jm} a_{jm}^*. \quad (76)$$

This estimator is clearly unbiased, $\langle \mathcal{E}(\bar{C}_l) \rangle = \bar{C}_l$, and it is very likely that this is also the best one although a rigorous proof is not presented here. Its variance can be expressed as

$$\sigma_{\mathcal{E}(\bar{C}_l)}^2 = \frac{1}{(2L+1)^2} \sum_{j=l-L}^{l+L} j^2(j+1)^2 \frac{2C_j^2}{2j+1}. \quad (77)$$

Using that $l(l+1)C_l \approx \text{const}$, if L is not too big, we arrive at

$$e_{\bar{C}_l}^{(\text{cv})} \equiv \frac{\sigma_{\mathcal{E}(\bar{C}_l)}}{\bar{C}_l} \times 100\% \approx \frac{1}{2L+1} \sqrt{\sum_{j=l-L}^{l+L} \frac{2}{2j+1}} \times 100\%. \quad (78)$$

For $L=0$ this error reduces to the known expression for the cosmic variance (74). In this case it is independent of the spectral index, whereas for $L \neq 0$ this is true as long as $l(l+1)C_l$ is approximately constant within the range $[l-L, l+L]$. With the same approximation we find that the slow-roll error in \bar{C}_l is just $e_{\bar{C}_l}^{(i)} \approx e_{C_l}^{(i)}$.

The cosmic variance for different multipoles and binning is displayed in table I. For comparison we give the errors in the multipole moments from the slow-roll approximation at leading and next-to-leading order for the pivot scale corresponding to the present horizon and we also present the errors at the next-to-leading order for the pivot scale corresponding to the scale of the first acoustic peak. We present the results for two values of the spectral index, corresponding to $1(2)\sigma$ errors in the COBE measurement.

For $k_0 = r_{\text{ISS}}^{-1}$, the error from the slow-roll approximation in leading order dominates over the cosmic variance already at $l=10$ for $n_S = 0.9$ and $L=0$. For the next-to-leading order and $n_S = 0.9$ the slow-roll error dominates over the cosmic variance at $l=100$, for any binning of multipoles. In the case of $n_S = 0.6$ only the error in the quadrupole from the slow-roll approximation at next-to-leading order is smaller than the cosmic variance. Only for $|n_S - 1| < 10^{-2}$ the error from the next-to-leading order is below 1%, which is the order of magnitude of the cosmic variance in the Silk damping regime of the spectrum.

For $k_0 = 1/22h^{-1}\text{Mpc}$, the situation is improved. The slow-roll error and the cosmic variance are of the same order of magnitude up to $l=1000$ ($n_S = 0.9$). However, this is not sufficient to hide the slow-roll error in the cosmic variance for the whole spectrum. For $n_S = 0.6$, the slow-roll error exceeds the cosmic variance at small and large scales and is hidden in the cosmic variance only for a narrow range of scales around k_0 . Let us point out that values of the tilt of the order of 0.1 and larger are a realistic possibility, as is clearly seen from the maximum likelihood fits to the recent BOOMERanG and MAXIMA-1 data.

We conclude that for a general model of inflation only numerical mode-by-mode integration can presently provide predictions for the CMBR with less than 1% error, unless all slow-roll parameters are less than 10^{-2} . To give an example let us consider the case of chaotic inflation with a potential $V \propto \varphi^p$, for which the slow-roll parameters are $\epsilon \approx p/200$, $\delta \approx (p-2)/200$, and $\xi \approx (p-2)(p-4)/(200p)$, giving $n_S^{(\text{sr})} \approx 1 - (p+2)/100$. Thus for $p = 2(4)$ the errors from the slow-roll approximation at next-to-leading order are of the same order

as the cosmic variance for large l , since $\epsilon \approx 0.01(0.02)$ and $\delta \approx 0(0.01)$, which corresponds to $n_S^{(\text{sr})} \approx 0.96(0.94)$. However, already for $p = 6$, the slow-roll approximation in the next-to-leading order leads to errors that exceed the cosmic variance at high multipoles ($\epsilon \approx 0.03$, $\delta \approx 0.02$, $\xi \approx 0.007$, thus $n_S^{(\text{sr})} \approx 0.92$).

Forthcoming high precision missions, especially the MAP and Planck satellites, will only be limited by the cosmic variance up to $l \approx 1000$ and $l \approx 2000$ respectively. Therefore predictions from inflationary models should be made such that the slow-roll error does not exceed the cosmic variance. We have shown that there are slow-roll models which cannot meet this requirement.

Another implication is that the large errors in the predicted multipoles render all attempts to reconstruct the inflationary potential difficult. The reason for this is that reconstruction usually assumes that the primordial spectrum, instead of the multipoles, is measured to a high precision. We have shown in this work, that the errors in the prediction of the multipoles are easily an order of magnitude larger. A first attempt to go directly from inflation to the calculation of the multipole moments has been put forward by Grivell and Liddle [38] recently. In our opinion a purely numerical approach to this fundamental issue is not fully satisfactory — better analytic methods are needed.

n_S	L	l	$e_{\bar{C}_l}^{(\text{cv})}$	$e_{\bar{C}_l}^{(0)}$	$e_{\bar{C}_l}^{(1)}$	$e_{\bar{C}_l}^{\text{impr}}$		
0.9	0	2	63%	15%	0.4%	8.1%		
		10	31%	34%	3.4%	4.1%		
		100	10%	68%	15%	0.35%		
		1000	3.2%	—	39%	1.0%		
		2	10	14%	34%	3.4%	4.1%	
			100	4.5%	68%	15%	0.35%	
	0.6	0	2	63%	73%	8.6%	56%	
			10	31%	—	92%	36%	
			100	10%	—	—	4.6%	
			1000	3.2%	—	—	22%	
			2	10	14%	—	92%	36%
				100	4.5%	—	—	4.6%
0.6	4	10	11%	—	92%	36%		
		100	3.3%	—	—	4.6%		
		1000	1.1%	—	—	22%		

TABLE I. Comparison of errors from the cosmic variance and the slow-roll approximation in leading and next-to-leading order with $k_0 r_{\text{ISS}} = 1$ and in next-to-leading order with $k_0 r_{\text{ISS}} = 100e$, for various values of the spectral index n_S , the bin width L , and the multipole l . The “—” denotes errors that exceed 100%.

ACKNOWLEDGMENTS

We would like to thank A. R. Liddle, V. F. Mukhanov, and V. Shani for valuable discussions and/or comments and an anonymous referee for suggesting to change the pivot scale. D. S. thanks the Austrian Academy of Sciences for financial support. J. M. thanks Robert Brandenberger and the High Energy Group of Brown University (Providence, USA) and the Institute für Theoretische Physik (Vienna, Austria) for warm hospitality.

-
- [1] P. de Bernadis et al., *Nature* **404**, 955 (2000); A. E. Lange et al., astro-ph/0005004 (2000); Boomerang <http://oberon.roma1.infn.it/boomerang/>.
- [2] S. Hanany et al., astro-ph/0005123 (2000); A. Balbi et al., astro-ph/0005124 (2000); Maxima-1 <http://cfpa.berkeley.edu/group/cmb/>.
- [3] MAP (Microwave Anisotropy Probe) <http://map.gsfc.nasa.gov/>; Planck <http://astro.estec.esa.nl/SA-general/Projects/Planck/>.
- [4] A. Guth, *Phys. Rev. D* **23**, 347 (1981); A. Linde, *Phys. Lett. B* **108**, 389 (1982); A. Albrecht and P. J. Steinhardt, *Phys. Rev. Lett.* **48**, 1220 (1982); A. Linde, *Phys. Lett. B* **129**, 177 (1983).
- [5] A. A. Starobinsky, *Pis'ma Zh. Eksp. Teor. Fiz.* **30**, 719 (1979) [*JETP Lett.* **30**, 682 (1979)].
- [6] V. Mukhanov and G. Chibisov, *JETP Lett.* **33**, 532 (1981); S. Hawking, *Phys. Lett.* **115B**, 295 (1982); A. A. Starobinsky, *Phys. Lett.* **117B**, 175 (1982); J. M. Bardeen, P. J. Steinhardt, and M. S. Turner, *Phys. Rev. D* **28**, 679 (1983).
- [7] A. Guth and S. Y. Pi, *Phys. Rev. Lett.* **49**, 1110 (1982).
- [8] V. F. Mukhanov, H. A. Feldman and R. H. Brandenberger, *Phys. Rep.* **215**, 203 (1992).
- [9] I. J. Grivell and A. R. Liddle, *Phys. Rev. D* **54**, 7191 (1996).
- [10] E. D. Stewart and D. H. Lyth, *Phys. Lett. B* **302**, 171 (1993).
- [11] L. Wang, V. F. Mukhanov and P. J. Steinhardt, *Phys. Lett. B* **414**, 18 (1997).
- [12] J. E. Lidsey et al., *Rev. Mod. Phys.* **69**, 373 (1997).
- [13] E. J. Copeland et al., *Phys. Rev. D* **49**, 1840 (1994).
- [14] E. W. Kolb and S. L. Vadas, *Phys. Rev. D* **50**, 2479 (1994).
- [15] E. J. Copeland et al., *Phys. Rev. D* **58**, 043002 (1998).
- [16] A. A. Starobinsky, talk at DARC, Meudon, December 11, 1998.
- [17] J. A. Bardeen, *Phys. Rev. D* **22**, 1882 (1980).
- [18] L. P. Grishchuk, *Zh. Eksp. Teor. Fiz.* **64**, 825 (1974) [*Sov. Phys. JETP* **40**, 409 (1974)].
- [19] V. F. Mukhanov, *Zh. Eksp. Teor. Fiz.* **94**, 1 (1988) [*Sov. Phys. JETP* **68**, 1297 (1988)].
- [20] L. P. Grishchuk, *Phys. Rev. D* **50**, 7154 (1994).
- [21] J. Martin and D. J. Schwarz, *Phys. Rev. D* **57**, 3302 (1998).
- [22] G. Smoot et al., *Astrophys. J.* **396**, L1 (1992); C. L. Bennett et al., *Astrophys. J.* **464**, L1 (1996); K. M. Gorski et al., *Astrophys. J.* **464**, L11 (1996).
- [23] R. K. Sachs and A. M. Wolfe, *Astrophys. J.* **147**, 73 (1967).
- [24] D. J. Fixsen et al., *Astrophys. J.* **473**, 576 (1996).
- [25] L. P. Grishchuk and J. Martin, *Phys. Rev. D* **56**, 1924 (1997).
- [26] P. J. E. Peebles, *Ap. J.* **263**, L1 (1982). J. R. Bond and G. Efstathiou, *Ap. J.* **285**, L45 (1984).
- [27] A. A. Starobinsky, *Sov. Astron. Lett.* **11**, 133 (1985).
- [28] R. L. Davis et al., *Phys. Rev. Lett.* **69**, 1856 (1992). D. S. Salopek, *Phys. Rev. Lett.* **69**, 3602 (1992). A. R. Liddle and D. H. Lyth, *Phys. Lett. B* **291**, 391 (1992).
- [29] T. Souradeep and V. Sahni, *Mod. Phys. Lett.* **7**, 3541 (1992).
- [30] R. Crittenden et al., *Phys. Rev. Lett.* **71**, 324 (1993).
- [31] P. J. Steinhardt, *Int. J. Mod. Phys. A* **10**, 1091 (1995).
- [32] J. Bardeen et al., *Astrophys. J.* **304**, 15 (1986).
- [33] U. Seljak and M. Zaldarriaga, *Astrophys. J.* **469**, 437 (1996); CMBFAST Website: <http://www.sns.ias.edu/~matiasz/CMBFAST/cmbfast.html>.
- [34] E. Bunn and M. White, *Astrophys. J.* **480**, 6 (1997).
- [35] D. H. Lyth, *Phys. Rev. D* **31**, 1792 (1985).
- [36] D. J. Schwarz and J. Martin, astro-ph/9805313 published in: *Current Topics in Mathematical Cosmology*, Eds. M. Rainer and H.-J. Schmid (World Scientific PC, Singapore, 1998) pp. 65.
- [37] A. Gangui and J. Martin, astro-ph/0001361.
- [38] I. J. Grivell and A. R. Liddle, *Phys. Rev. D* **61**, 081301 (2000).